Liquid-crystalline Casimir effect in the presence of a patterned substrate

F. Karimi Pour Haddadan*, F. Schlesener, and S. Dietrich

Max-Planck-Institut für Metallforschung,
Heisenbergstr. 3, D-70569 Stuttgart, Germany,
and
Institut für Theoretische und Angewandte Physik,
Universität Stuttgart, Pfaffenwaldring 57,
D-70569 Stuttgart, Germany
(Dated: February 2, 2008)

We consider a nematic liquid crystal confined by two parallel planar interfaces, one being laterally homogeneous and the other provided by a substrate endowed with a periodic chemical stripe pattern. Based on continuum theory we analyze the influence of the lateral pattern on the liquid-crystalline Casimir force acting on the interfaces of the nematic cell at distance d due to the thermal fluctuations of the nematic director. For d much larger than the pattern periodicity, the influence of the patterned substrate can be described by a homogeneous, effective anchoring energy. By tuning this parameter we recover previous results for the liquid-crystalline Casimir force. For the general case, i.e., smaller separations, we present new numerical results.

PACS numbers: 61.30.Dk, 61.30.Hn

I. INTRODUCTION

Liquid crystals in general are sensitive over a wide spatial range to the anchoring conditions of confining interfaces. This holds also for lateral variations of anchoring conditions generated either by surface topography [1, 2, 3, 4, 5, 6, 7] or patterning [8, 9, 10, 11, 12, 13, 14, 15, 16, 17, 18] giving rise to numerous possible applications. In recent years, the influence of the structured substrates on the properties of liquid crystals has been studied and it has been demonstrated that to a certain extent such nontrivial geometries may optimize the performance of electro-optical liquid-crystalline devices. For instance, a four-domain twisted nematic liquid crystal display provides a wide viewing angle with no gray scale inversion[19] and using multistable nematic liquid-crystal devices with micropatterned substrate alignments reduces the energy consumption [4, 6, 13, 15].

The influence of the anchoring on the liquid crystal order parameter translates into an effective interaction between the confining interfaces which may be provided either by true solid substrates or by an adjacent vapor phase where the former case can support permanent lateral structures. Here we consider liquid crystals deep in their nematic phase where the orientational order is described by a director field with long-ranged correlations. In case of any mismatch between the prescribed alignment of the bulk and the substrates, the director structure may not be uniform. In such a case, the free energy of the system typically exhibits several, metastable, minima which upon a change in the parameters of the system – such as the film thickness, external, or internal forces – may turn into the global minimum resulting in a structural phase transition [20]. This makes the stability of the equilibrium configuration geometry dependent. In this context one should keep in mind that perturbative

approaches may miss the occurrence of first-order structural phase transition. We shall consider the case of frustrated systems in which, however, the director structure remains uniform up to a critical thickness d_c. Within such a regime the liquid-crystalline mediated effective interaction between the confining interfaces due to the thermal fluctuations of the director adds to background contributions due to structural forces arising from presmectic layering [21, 22, 23] and enhanced ordering near the substrates [21] and due to dispersion forces [24] which exhibit only a weak temperature dependence.

Using the continuum Frank free energy, we study the fluctuation-induced interaction – the so-called liquid-crystalline Casimir effect – between two parallel interfaces where one is periodically patterned and the other one is homogeneous. We consider a periodicity in the local anchoring energy and model the liquid crystal-substrate interaction by the Rapini-Papoular surface free energy. We investigate the modification of the fluctuation-induced force compared with its behavior for substrates with uniform anchoring conditions [25] as a function of the pattern periodicity ζ and the characteristic length of the pattern ζ_a (see Fig. 1).

Two model systems are considered. One consists of a substrate with a pattern characterized by homeotropic anchoring of alternating strengths facing a second substrate at a distance d which is characterized by a uniformly strong homeotropic anchoring. For this system the mean director is constant at any separation. By changing the boundary condition via the change of the patterning ratio ζ_a/ζ, the character of the force changes. Depending on whether the boundaries are effectively similar-nonsimilar or similar-similar the force is repulsive or attractive, respectively. For certain values of ζ_a/ζ and of the reduced distance d/ζ, the liquid-crystalline Casimir force vanishes. In the second system the pattern

consists of alternating stripes of homeotropic and degenerate planar anchoring while the upper substrate still exhibits strong homeotropic anchoring. In this case there is the possibility of texture formation [16]. However, for separations smaller than a critical one the director structure is indeed uniform [26]. For those ranges of the model parameters for which the director is constant (see, c.f., Subsec. III B), we find a nonmonotonic behavior for the fluctuation-induced force.

There are several techniques that can be used to create periodic anchoring conditions such as photo-alignment [15], the selectively thiol-functionalized photo-orientation [16], and atomic force lithography [11]. In the latter case patterning at the nano-meter scale is reached which allows one to investigate more efficiently the influence of the patterned substrate on the liquid crystal. The results of our study, for example, might be helpful in designing thin patterned liquid crystalline films for which the fluctuation-induced force plays a role for the stability of the film.

In Sec. II we describe the system and the formalism that we apply for calculating the fluctuation induced effective interaction. In Subsec. III A we investigate the force in the presence of a pattern of alternating anchoring strengths and in Subsec. III B with a pattern of competing anchoring conditions. We present analytical results for patterns of small and large scales and numerical results for patterns at intermediate scales. In Sec. IV we summarize our results.

II. SYSTEM AND THEORETICAL MODEL

We consider a liquid crystal in a nematic phase and confined by two parallel planar interfaces at a distance d (see Fig. 1). The liquid crystal is described by the Frank free energy [27]

$$F = \frac{1}{2} \int_V \mathrm{d}^3 x \Big[K_1 (\boldsymbol{\nabla} \cdot \mathbf{n})^2 + K_2 (\mathbf{n} \cdot \boldsymbol{\nabla} \times \mathbf{n})^2$$
$$+ K_3 (\mathbf{n} \times \boldsymbol{\nabla} \times \mathbf{n})^2 \Big], \quad (1)$$

where $\mathbf{n}$ denotes the director of the liquid crystal, V is the nematic volume, and K_1, K_2, and K_3 are the splay, the twist, and the bend elastic constants, respectively. The interaction between the liquid crystal and the substrate is modeled by the Rapini-Papoular surface free energy [28] given by

$$F_s = -\frac{1}{2} \int_A \mathrm{d}^2 x \, W(\mathbf{x}) \, (\mathbf{n} \cdot \mathbf{e})^2, \quad (2)$$

where $\mathbf{x} = (x, y)$ denotes the lateral coordinates of Cartesian coordinates $\mathbf{r} = (\mathbf{x}, z)$, A is the surface area, W is the anchoring energy per area, and $\mathbf{e}$ is the easy direction, i.e., the preferred direction of the director at the substrate if $W > 0$. For $W < 0$ the director prefers the direction perpendicular to $\mathbf{e}$. In the following we restrict the discussion to the case that $\mathbf{e}$ is perpendicular
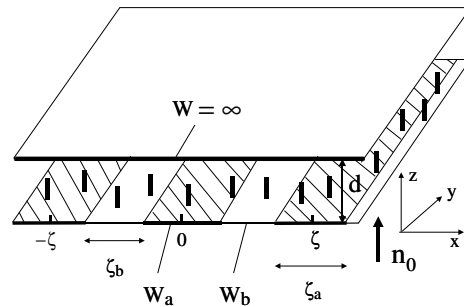

FIG. 1: The geometry of the nematic cell with cross section A and volume $V = Ad$. The upper boundary is characterized by strong homeotropic anchoring. The lower substrate is patterned. The pattern consists of periodic stripes of anchoring energies per area W_a and W_b with widths ζ_a and ζ_b, respectively, so that $\zeta = \zeta_a + \zeta_b$. The easy directions (see Eq. (2)) at both boundaries are normal to the interfaces and we consider such values of W_a and W_b for which the thermal average of the director field $\mathbf{n}_0$ is homogeneous.

to both substrates, which leads to homeotropic anchoring for $W > 0$ and to degenerate (i.e., with no preferred azimuthal angle) planar anchoring for $W < 0$.

On the lower substrate located at $z = 0$, we assume that the anchoring energy varies periodically along the x-direction. The pattern consists of alternating stripes of anchoring energies per area W_a and W_b. The substrate remains translationally invariant in the y-direction. On the upper substrate located at $z = d$ we assume uniformly strong homeotropic anchoring (see after, c.f., Eq. (9)).

In general, the local director field is given by

$$\mathbf{n}(\mathbf{x}, z) = \mathbf{n}_0(\mathbf{x}, z) + \boldsymbol{\delta}(\mathbf{x}, z) \quad (3)$$

where $\mathbf{n}_0(\mathbf{x}, z)$ is the thermal average of the director and $\boldsymbol{\delta}(\mathbf{x}, z)$ is the fluctuating part with vanishing thermal average $\langle \boldsymbol{\delta} \rangle = 0$.

A. Mean-field behavior

First we discuss the mean-field solution $\mathbf{n}_0(\mathbf{x}, z)$ of the director field. In the case of homeotropic anchoring everywhere on the lower substrate, the uniform solution $\mathbf{n}_0 = (0, 0, 1)$ is the equilibrium configuration. On the other hand in case of planar anchoring everywhere on the lower substrate, the liquid crystal is subject to competing surface interactions at the top and the bottom. For this so-called hybrid cell – a cell with uniform homeotropic and uniform planar anchoring on each substrate – it has been shown that the substrate whose anchoring is stronger can impose a uniform director configuration up to a critical separation between the plates [29].

In the case of periodic pattern of homeotropic and planar anchoring on the substrate (Subsec. III B), the full phase diagram of the system within mean field theory and the structural phase transition between a uniform director configuration and a distorted one can be studied by means of numerical minimization of the free energy functional [14, 26]. However, one can naively expect that in this system the tendency to form a uniform director field is enhanced with respect to the hybrid cell due to the presence of the interlaced homeotropic stripes. In the following we restrict the discussion to separations smaller than the critical separation d_c for which the director configuration is uniform and focus on the fluctuations.

B. Fluctuations of the director

Next we consider fluctuations around the uniform director $\mathbf{n}_0 = (0, 0, 1)$. Since the director $\mathbf{n}(\mathbf{x}, z)$ is a unit vector the fluctuations can be described by $\boldsymbol{\delta} = (\delta_x, \delta_y, -1 + \sqrt{1 - \delta_x^2 - \delta_y^2}) \simeq (\delta_x, \delta_y, -\delta_x^2/2 - \delta_y^2/2)$, where $\delta_x(\mathbf{x}, z)$ and $\delta_y(\mathbf{x}, z)$ are the two independent components. According to Eq. (1) and within the one-constant approximation, the bulk contribution to the statistical weight $\exp(-\beta \mathcal{H}_{\mathrm{bulk}}[\mathbf{n}])$ for a director configuration $\mathbf{n}$ is given by $\mathcal{H}_{\mathrm{bulk}}[\mathbf{n}] = \mathcal{H}_{\mathrm{bulk}}[\delta_x] + \mathcal{H}_{\mathrm{bulk}}[\delta_y]$ with

$$\mathcal{H}_{\mathrm{bulk}}[\nu] = \frac{K}{2} \int_V \mathrm{d}^3 x \left[\nabla \nu(\mathbf{x}, z) \right]^2, \tag{4}$$

where $\beta^{-1} = k_B T$ is the thermal energy and K is the effective elastic constant [30]. Eq. (4) amounts to considering Gaussian fluctuations, i.e., the Hamiltonian is quadratic in $\nu(\mathbf{x}, z)$. This is expected to give a qualitatively correct description of the system except near an incipient structural phase transition.

As a local contribution the surface interaction is evaluated at the interfaces $z = 0$, $z = d$. The lower substrate is characterized by the patterning function

$$a(x) = \sum_{k=-\infty}^{\infty} \Theta\left(x - k\zeta + \frac{\zeta_a}{2} \right) \Theta\left(k\zeta + \frac{\zeta_a}{2} - x \right), \tag{5}$$

where $\Theta(x)$ is the Heaviside step function, ζ is the periodicity, ζ_a is the width of the stripe characterized by W_a, and $\zeta_b = \zeta - \zeta_a$ is the width of the stripe characterized by W_b (Fig. 1). The stripes form sharp chemical steps between them. The function $a(x)$ is one at the regions characterized by W_a and zero elsewhere. Accordingly, for this model the surface interaction [Eq. (2)] disregarding constant terms is given by $\mathcal{H}_{\mathrm{surf}}[\mathbf{n}] = \mathcal{H}_{\mathrm{surf}}[\delta_x] + \mathcal{H}_{\mathrm{surf}}[\delta_y]$ with

$$\mathcal{H}_{\mathrm{surf}}^{z=0}[\nu] = \frac{1}{2} \Big[W_a \int_A \mathrm{d}^2 x \left(\nu(\mathbf{x}, z=0) \right)^2 a(x)$$
$$+ W_b \int_A \mathrm{d}^2 x \left(\nu(\mathbf{x}, z=0) \right)^2 (1 - a(x)) \Big] \tag{6}$$

for the lower substrate. We assume homogeneous anchoring on the upper boundary so that

$$\mathcal{H}_{\mathrm{surf}}^{z=d}[\nu] = \frac{1}{2} W \int_A \mathrm{d}^2 x \left(\nu(\mathbf{x}, z=d) \right)^2. \tag{7}$$

Minimization of the Hamiltonian $\mathcal{H}[\nu] = \mathcal{H}_{\mathrm{bulk}}[\nu] + \mathcal{H}_{\mathrm{surf}}^{z=0}[\nu] + \mathcal{H}_{\mathrm{surf}}^{z=d}[\nu]$ leads to the following boundary conditions:

$$- K \partial_z \nu(\mathbf{x}, z) + W_a \nu(\mathbf{x}, z)\, a(x)$$
$$+ W_b \nu(\mathbf{x}, z) \left(1 - a(x) \right) = 0,\ z = 0, \tag{8 a}$$

$$K \partial_z \nu(\mathbf{x}, z) + W \nu(\mathbf{x}, z) = 0,\ z = d, \tag{8 b}$$

where ν is either δ_x or δ_y. After integration by parts in Eq. (4) and using the boundary conditions given by Eqs. (8 a) and (8 b), the Hamiltonian $\mathcal{H}[\nu]$ reduces to $\mathcal{H}[\nu] = -\frac{K}{2} \int_V \mathrm{d}^3 x\, \nu(\mathbf{x}, z) \nabla^2 \nu(\mathbf{x}, z)$. In terms of the so-called extrapolation lengths λ_a and λ_b

$$\lambda_{a(b)} = \frac{K}{W_{a(b)}}, \tag{9}$$

the boundary condition [Eq. (8 a)] on the patterned substrate $z = 0$ reads $\mathcal{A}_1(\mathbf{x}, z) = -\lambda_b \partial_z \nu(\mathbf{x}, z) + \left(1 + \frac{\lambda_b - \lambda_a}{\lambda_a} a(x) \right) \nu(\mathbf{x}, z) = 0$. Assuming strong homeotropic anchoring $W = \infty$ ($\lambda = 0$) at the upper boundary, Eq. (8 b) leads to the Dirichlet boundary condition $\mathcal{A}_2(\mathbf{x}, z=d) \equiv \nu(\mathbf{x}, z=d) = 0$.

As an aside, we note the relation between the present model and those for surface critical phenomena. Rescaling the fluctuating field by $K/k_B T$, the Hamiltonian in Eq. (4) can be written as $\mathcal{H}_b[\varphi] = k_B T \int_V \mathrm{d}^3 x\, \frac{1}{2}(\nabla \varphi)^2$ and the surface interaction in Eq. (7) is represented by $\mathcal{H}_S[\varphi] = k_B T \int_A \mathrm{d}^2 x\, \frac{c}{2} \varphi^2$, where $c = W/K$ is the inverse extrapolation length of the critical order parameter profile at a surface [31]. The limiting cases $c = \infty$ and $c = 0$ correspond to Dirichlet and v. Neumann boundary conditions, respectively. The bulk Hamiltonian for a system close to the critical point also includes the terms $\frac{\tau}{2}\varphi^2$ and $\frac{u}{24}\varphi^4$ of which the former one vanishes at the critical point. In this sense the present study corresponds to discussing, within the Gaussian approximation, a slab of a system at bulk criticality confined by planar surfaces one of them endowed with a pattern of the extrapolation length.

C. The fluctuation-induced force

We employ the path integral method introduced by Li and Kardar for calculating the partition function of the system [32, 33] which amounts to integrate over all configurations of the fluctuating field weighted by the Boltzmann factor and subject to the boundary conditions. We

impose the boundary conditions by inserting delta functions into the path integral. Thus the partition function Z of the field ν reads

$$Z = \int \mathcal{D}\nu(\mathbf{r}) \; e^{-\mathcal{H}[\nu]/(k_BT)}$$
$$\times \prod_{\mathbf{x}} \delta\Big(\mathcal{A}_1(\mathbf{x}, z=0)\Big)\prod_{\mathbf{x}}\delta\Big(\mathcal{A}_2(\mathbf{x}, z=d)\Big) \quad (10)$$

with the functional integral defined via a discretization on a lattice $\{\mathbf{r}_n\}$ in the limit of a vanishing lattice constant: $\int \mathcal{D}\nu(\mathbf{r}) \equiv \prod_n \int_{-\infty}^{\infty} \frac{d\nu(\mathbf{r}_n)}{\sqrt{2\pi}}$ [34]. Using the integral representation of the delta function,

$$\prod_{\mathbf{x}}\delta\Big(\mathcal{A}_\alpha(\mathbf{x})\Big) = \int \mathcal{D}\Psi_\alpha \exp\left(i\int d^2x\, \Psi_\alpha\, \mathcal{A}_\alpha\right), \, \alpha = 1,2, \quad (11)$$

and performing the Gaussian integral over the field ν, we obtain

$$Z = \mathcal{N}\int \prod_{\alpha=1}^{2}\mathcal{D}\Psi_\alpha\; e^{-\mathcal{H}_{\text{eff}}}, \quad (12)$$

where $\Psi_{\alpha=1,2}$ are auxiliary fields defined at $z=0$ and $z=d$, respectively, $\mathcal{N}$ is a factor independent of d, and the effective interaction reads

$$\mathcal{H}_{\text{eff}} = \sum_{\alpha,\beta=1}^{2}\int d^2x \int d^2x' \Psi_\alpha(\mathbf{x})M_{\alpha,\beta}(\mathbf{x},\mathbf{x}')\Psi_\beta(\mathbf{x}'), \quad (13)$$

where M is regarded as a matrix both with respect to the indices α, β and the coordinates $\mathbf{x}$, $\mathbf{x}'$:

$$M_{11}(\mathbf{x},\mathbf{x}') = \left\{[1+\tfrac{\lambda_b-\lambda_a}{\lambda_a}a(x)][1+\tfrac{\lambda_b-\lambda_a}{\lambda_a}a(x')] + \tfrac{\lambda_b(\lambda_b-\lambda_a)}{\lambda_a}[a(x)-a(x')]\partial_z - \lambda_b^2\partial_z^2\right\}G(\mathbf{x}-\mathbf{x}',z-z')\Big|_{z=z'=0}$$
$$M_{12}(\mathbf{x},\mathbf{x}') = \left(1+\tfrac{\lambda_b-\lambda_a}{\lambda_a}a(x')-\lambda_b\partial_{z'}\right)G(\mathbf{x}-\mathbf{x}',z-z')\Big|_{z=d,z'=0}$$
$$M_{21}(\mathbf{x},\mathbf{x}') = \left(1+\tfrac{\lambda_b-\lambda_a}{\lambda_a}a(x)-\lambda_b\partial_z\right)G(\mathbf{x}-\mathbf{x}',z'-z)\Big|_{z'=d,z=0}$$
$$M_{22}(\mathbf{x},\mathbf{x}') = G(\mathbf{x}-\mathbf{x}',z-z')\Big|_{z=z'=d} \quad (14)$$

where $G(\mathbf{r},\mathbf{r}') = \frac{k_BT}{4\pi K|\mathbf{r}-\mathbf{r}'|}$ is the bulk two-point correlation function in three dimensions defined by $\frac{K}{k_BT}\nabla^2 G(\mathbf{r}-\mathbf{r}') = -\delta(\mathbf{r}-\mathbf{r}')$.

Due to the symmetries in the xy-plane it is useful to switch to the Fourier transformed quantities. We note that if the patterning function $a(x) = 1$, i.e., for a homogeneous substrate ($\lambda_a = \lambda_b$), the matrix M is diagonal in the lateral Fourier space $(\mathbf{p},\mathbf{q})$. However, here the patterning function is piecewise either one or zero [Eq. (5)]. Due to the periodicity of the patterning along the x-direction, i.e., $a(x) = a(x+\zeta)$,

and the translational invariance along the y-direction, the matrix M in the lateral Fourier space, $M(\mathbf{p},\mathbf{q}) = \int\int d^2x\, d^2x' M(\mathbf{x},\mathbf{x}')e^{i\mathbf{p}\cdot\mathbf{x}}e^{i\mathbf{q}\cdot\mathbf{x}'}$, has the following form:

$$M(\mathbf{p},\mathbf{q}) = (2\pi)^2\delta(p_y+q_y)\sum_{m=-\infty}^{\infty}N_m(p_x,p_y)$$
$$\times\delta\left(p_x+q_x+\frac{2\pi m}{\zeta}\right) \quad (15)$$

with the (2×2) matrices N_m given by

$$N_0 = \begin{pmatrix} [(1+\tfrac{\lambda_b-\lambda_a}{\lambda_a}\tfrac{\zeta_a}{\zeta})^2-\lambda_b^2\partial_z^2]G(p,z-z')\big|_{z=z'=0}+\phi_0 & (1+\tfrac{\lambda_b-\lambda_a}{\lambda_a}\tfrac{\zeta_a}{\zeta}-\lambda_b\partial_{z'})G(p,z-z')\big|_{z=d,z'=0} \\ (1+\tfrac{\lambda_b-\lambda_a}{\lambda_a}\tfrac{\zeta_a}{\zeta}-\lambda_b\partial_z)G(p,z'-z)\big|_{z'=d,z=0} & G(p,z-z')\big|_{z=z'=d} \end{pmatrix} \quad (16)$$

and

$$N_{m\neq0} = \begin{pmatrix} \tfrac{\lambda_b-\lambda_a}{\lambda_a}a_m[(1+\tfrac{\lambda_b-\lambda_a}{\lambda_a}\tfrac{\zeta_a}{\zeta})G(p,z-z')+G(\hat p_m,z-z')]\big|_{z=z'=0}+\phi_m & \tfrac{\lambda_b-\lambda_a}{\lambda_a}a_m G(p,z-z')\big|_{z=d,z'=0} \\ \tfrac{\lambda_b-\lambda_a}{\lambda_a}a_m G(\hat p_m,z'-z)\big|_{z'=d,z=0} & 0 \end{pmatrix} \quad (17)$$

with $p = \sqrt{p_x^2+p_y^2}$, $\hat p_m = \sqrt{(p_x+2\pi m/\zeta)^2+p_y^2}$, the two-point correlation function in lateral Fourier space

$$G(p,z-z') = \frac{k_BT}{2Kp}e^{-p|z-z'|}, \quad (18)$$

and

$$\phi_m = \left(\frac{\lambda_b-\lambda_a}{\lambda_a}\right)^2\sum_{k=-\infty}^{\infty}{}' a_k a_{m-k}G(\hat p_k,0) \quad (19)$$

where the prime at the summation sign indicates that in the sum the term $k = 0$ is excluded. The patterning function $a(x)$ is represented as a Fourier series $a(x) = \sum_{k=-\infty}^{\infty} a_k e^{2\pi i k x/\zeta}$ with

$$a_k = \frac{1}{L} \int_{-L/2}^{L/2} dx\, a(x) \exp(-2\pi i k x/\zeta) = \frac{1}{\pi k} \sin(\pi k \zeta_a/\zeta), \quad (20)$$

where L is the extension of the system along the x−direction (see Fig. 1). We mention that the patterning function $a(x)$ is coordinate dependent and the phase of the coefficients a_k depends on the choice of the position of the coordinate origin used for a(x), but as expected the final result for the force is independent of this choice. We have checked this numerically [c.f., Eq. (25)].

Each pair of the momenta $(\mathbf{p}, \mathbf{q})$ indicates one element of the matrix M which is a (2×2) matrix itself [Eq. (15)]. Although M has an infinite number of elements and is not diagonal it can be brought into a block

diagonal form by an even number of row and column permutations [35, 36]. We take the system to be periodically extended with period $L = N\zeta$ along the x-axis with N being an integer. This leads to momenta p_x that are integer multiples of $2\pi/L$. For p_x fixed the factor $\delta(p_x + q_x + 2\pi m/\zeta)$ in Eq. (15) leads to nonvanishing matrix elements for all $q_x = -p_x - 2\pi m/\zeta$ with $m \in \mathbb{Z}$. This allows one to identify the block structure of the matrix M. For fixed j the momenta $p_x = 2\pi j/L + 2\pi l/\zeta$ and $q_x = -2\pi j/L - 2\pi k/\zeta$ form the block M_j where $l, k \in \mathbb{Z}$ and $j = 1, \cdots, N = L/\zeta$ so that there is no multiple counting of the momenta. One can read off the elements of the infinite-dimensional block matrices $M_j(p_y, q_y)$ from Eq. (15):

$$M_{j,kl}(p_y, q_y) = 2\pi\, \delta(p_y + q_y)\, B_{kl}\left(\frac{2\pi j}{L}, p_y\right) \quad (21)$$

with the matrix B given by

$$B\left(p_x = \frac{2\pi}{L} j\right) = \begin{pmatrix} \ddots & & \vdots & & \iddots \\ & N_0(p_x - \frac{2\pi}{\zeta}) & N_{-1}(p_x) & N_{-2}(p_x + \frac{2\pi}{\zeta}) & \\ \cdots & N_1(p_x - \frac{2\pi}{\zeta}) & N_0(p_x) & N_{-1}(p_x + \frac{2\pi}{\zeta}) & \cdots \\ & N_2(p_x - \frac{2\pi}{\zeta}) & N_1(p_x) & N_0(p_x + \frac{2\pi}{\zeta}) & \\ \iddots & & \vdots & & \ddots \end{pmatrix}, \quad (22)$$

so that the matrix element B_{kl} reads

$$B_{kl}\left(\frac{2\pi j}{L}, p_y\right) = N_{m=k-l}\left(\frac{2\pi j}{L} + \frac{2\pi l}{\zeta}, p_y\right). \quad (23)$$

Note that a reindexation of the (p_y, q_y)-subspace is not necessary as M is diagonal with respect to it [Eq. (15)].

Now the value of the path integral [Eq. (12)] given by

$$Z = \mathcal{N}(det\, M)^{-1/2} \quad (24)$$

can be calculated in Fourier space. The free energy $-k_B T \ln Z$ of the system usually lends itself to a decomposition into bulk, surface, and finite-size contributions [37]. The term $-k_B T \ln \mathcal{N}$ leads to the bulk free energy. The factor $\mathcal{N}$ introduced in Eq. (12) is given by $\mathcal{N} = [det\, G^{-1}(\mathbf{r}, \mathbf{r}')]^{-1/2}$ where the determinant of the inverse of the two-point correlation function $G(\mathbf{r} - \mathbf{r}')$ in an unperturbed nematic is calculated in the space actually occupied by the nematic, i.e., the volume V. Thus the result for the bulk free energy is given by $F_{\text{bulk}} = k_B T V \int_0^{Q_{max}} \frac{dQ}{(2\pi)^2} Q^2 \ln\left(\frac{KQ_{\max}^{-3}Q^2}{k_B T}\right)$ where $Q_{\max}$ is an ultraviolet momentum cutoff of the order of the inverse size of the nematic molecules. The remaining part of the free energy $F = A(F_{\text{surf}}^{z=0} + F_{\text{surf}}^{z=d}) + \delta F(d)$ is given by $F = \frac{k_B T}{2} \ln \det M$. Here the d-independent terms $F_{\text{surf}}^{z=0}$

and $F_{\text{surf}}^{z=d}$ are the surface tensions associated with the interfaces at $z = 0$ and $z = d$, respectively, and the finite-size contribution $\delta F(d)$ is the fluctuation-induced interaction. In the present model there are no other finite-size contributions. Using the block structure of M, we obtain $\ln \det M = \ln(\prod_{j=1}^{N} \det M_j) = \sum_{j=1}^{N} \ln(\det M_j)$. Thus the fluctuation-induced force $\mathcal{F} = -\partial_d F$ equals $\mathcal{F} = -\frac{k_B T}{2} \sum_{j=1}^{N} \text{Tr}(M_j^{-1} \partial_d M_j)$. The final result for the force reads

$$\mathcal{F} = -\frac{k_B T A}{2\pi^2} \int_0^{\infty} dp_y \int_0^{2\pi/\zeta} dp_x$$
$$\times \text{Tr}\left(B^{-1}(p_x, p_y)\partial_d B(p_x, p_y)\right), \quad (25)$$

where we have carried out the thermodynamic limit $L \to \infty$ so that the summation over j is replaced by $\frac{L}{2\pi} \int_0^{2\pi/\zeta} dp_x$. The trace over the continuous momenta p_y is also replaced by $\frac{L}{\pi} \int_0^{\infty} dp_y$ and $A = L^2$. Equation (25) takes also into account that there are two independent fluctuating fields ν (i.e., δ_x and δ_y) which lead to a doubling of the force. Note that in Eq. (25) the trace is taken with respect to the remaining discrete indices k and l [Eq. (23)]. This can be calculated numerically by truncating the matrix B_{kl} at order I, i.e., $k, l = -(I-1)/2, \ldots, 0, \ldots, (I-1)/2$. The force $\mathcal{F}$ follows from extrapolating $I \to \infty$.

III. RESULTS

In the limit $d/\zeta \gg 1$ the contributions from the matrices N_m to $\det M$ decrease rapidly with increasing m [Eq. (15)]. In this limiting case it is sufficient to consider only the contribution from $N_0(p_x, p_y)$, in the sense that truncating the matrix B [Eq. (23)] at $I > 1$ leaves the integrand in Eq. (25) practically unchanged. Therefore it is instructive first to focus on this limiting case, which may correspond to a nano-patterned substrate facing a homogeneous substrate at a micrometer separation, and to investigate analytically the behavior of the force.

A. Pattern of different anchoring strengths

Here we consider a pattern characterized by stripes of homeotropic anchoring so that both W_a and W_b are positive. In this case the fluctuations are suppressed at the substrates [Eq. (6)]. Using Eqs. (23), (16), and (25) we find for the force

$$\mathcal{F}(\, d \gg \zeta) = \lim_{\zeta \to 0} \frac{-k_B T A}{2\pi^2} \int_0^\infty dp_y \int_0^{2\pi/\zeta} dp_x$$
$$\times \text{Tr}\left(N_0^{-1}(p_x, p_y)\partial_d N_0(p_x, p_y)\right)$$
$$= \frac{k_B T A}{\pi d^3} \int_0^\infty dx \frac{x^2}{\frac{x+d/\lambda_{\text{eff}}}{x-d/\lambda_{\text{eff}}}\exp(2x) + 1} \qquad (26)$$

where

$$\lambda_{\text{eff}} = \frac{\zeta \lambda_a \lambda_b}{\zeta_a \lambda_b + \zeta_b \lambda_a} \qquad (27)$$

is introduced as an effective extrapolation length and $x = pd$ is the rescaled momentum. Thus in the limit $d \gg \zeta$ the patterned substrate can be described by an effective anchoring energy per area with the force found between two homogeneous substrates where one substrate is characterized by strong anchoring and the other substrate is characterized by a finite anchoring, i.e., a finite extrapolation length λ_{eff} [38].

If λ_a or λ_b is zero, λ_{eff} vanishes and the force is long-ranged and attractive:

$$\mathcal{F}(d \gg \zeta, \lambda_{\text{eff}} = 0) = -\frac{k_B T A \zeta(3)}{4\pi d^3} \qquad (28)$$

where $\zeta(s) = \sum_{t=1}^\infty t^{-s}$ is the Riemann zeta function. This expression equals the one obtained for substrates both characterized by homogeneous strong anchoring [25]. This implies that in this limit the fluctuation-induced force is not affected by the stripes with weaker anchoring. This behavior resembles the one of the electrodynamic Casimir force between a flat and a rectangularly corrugated substrate [35] in the limiting
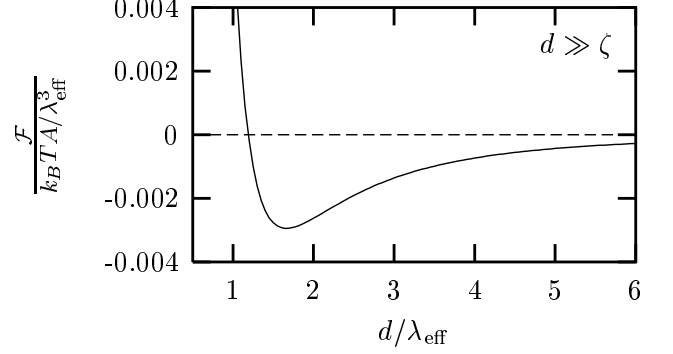

FIG. 2: The fluctuation-induced force $\mathcal{F}$ as a function of the reduced separation d/λ_{eff} in the case in which the patterned substrate can be described by an effective homeotropic anchoring ($d \gg \zeta$, see Eq. (26)). A crossover from repulsion to attraction occurs for a separation $d/\lambda_{\text{eff}} \simeq 1.19$ followed by a minimum at $(\frac{d}{\lambda_{\text{eff}}}, \frac{\mathcal{F}}{k_B T A/\lambda_{\text{eff}}^3}) \simeq (1.65, -0.003)$.

case that the periodicity is much smaller than the amplitude $2h$ of the corrugation and the mean separation H between the substrates. In this case the force equals the one between two flat substrates at a reduced mean separation $H - h$ so that the force is not affected by the valleys of the corrugated substrate.

At intermediate values of λ_{eff} there is a crossover from attraction to repulsion (Fig. 2). At separations smaller than $\lambda^* \simeq 1.19\,\lambda_{\text{eff}}$, the boundaries effectively act as being homogeneous but dissimilar – one boundary characterized by strong anchoring and the other boundary characterized by a finite weak anchoring so that the force is repulsive [39]. The asymptotic behavior of the force for $d/\lambda_{\text{eff}} \ll 1$ is given by

$$\mathcal{F}(\zeta \ll d \ll \lambda_{\text{eff}}) \approx \frac{3k_B T A \zeta(3)}{16\pi d^3}\left(1 - \frac{8\ln 2}{3\zeta(3)}\frac{d}{\lambda_{\text{eff}}}\right). \qquad (29)$$

Thus in this regime the leading long-ranged repulsion term $\sim d^{-3}$, corresponding to two homogeneous substrates characterized by infinitely strong and zero anchoring (Dirichlet-Neumann boundary conditions), is weakened. At separations larger than λ^*, the boundaries effectively act as being similar – one boundary characterized by infinitely strong and the other boundary characterized by finite yet strong anchoring; therefore the force is attractive [39]. The asymptotic behavior of the force for $d/\lambda_{\text{eff}} \gg 1$ is given by (compare Eq. (28))

$$\mathcal{F}(d \gg \lambda_{\text{eff}}, \zeta) \approx -\frac{k_B T A \zeta(3)}{4\pi d^3}\left(1 - \frac{3\lambda_{\text{eff}}}{d}\right). \qquad (30)$$

This means that the long-ranged attraction $\sim d^{-3}$, corresponding to two homogeneous substrates characterized by infinitely strong anchoring, is reduced. In Fig. 3 the amplitude of the fluctuation-induced force $\mathcal{F}(d \gg \zeta)$, as
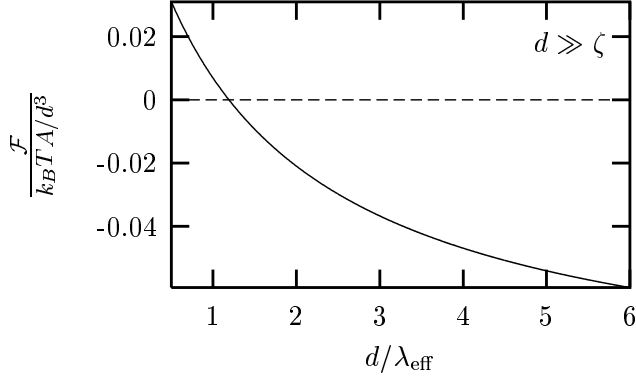
FIG. 3: Amplitude of the fluctuation-induced force $\mathcal{F}$ relative to asymptotic behavior d^{-3} as a function of the reduced separation d/λ_{eff} in the case in which the patterned substrate can be described by an effective homeotropic anchoring ($d \gg \zeta$, see Eq. (26)). At $d/\lambda_{\text{eff}} = 0$ this amplitude attains the value $3\zeta(3)/(16\pi) \simeq 0.072$ linearly [Eq. (29)] and approaches the value $-\zeta(3)/(4\pi) \simeq -0.096$ for $d/\lambda_{\text{eff}} \to \infty$ [Eq. (30)].

given by the full expression in Eq. (26), is shown as a function of the reduced separation d/λ_{eff}.

In Fig. 4 the force [Eq. (26)] is shown as a function of the patterning ratio ζ_a/ζ. Also in this case the above considerations provide an understanding of the crossover from repulsion to attraction upon changing the patterned substrate from the effectively weak to the effectively strong anchoring regime.

In the opposite limiting case $d/\zeta \ll 1$, the force is given by

$$
\mathcal{F}(d \ll \zeta) = \frac{k_B T A}{\pi d^3} \left(\frac{\zeta_a}{\zeta} \int_0^\infty \mathrm{d}x \frac{x^2}{\frac{x+d/\lambda_a}{x-d/\lambda_a} \exp(2x) + 1} \right.
$$
$$
\left. + \frac{\zeta_b}{\zeta} \int_0^\infty \mathrm{d}x \frac{x^2}{\frac{x+d/\lambda_b}{x-d/\lambda_b} \exp(2x) + 1} \right). \quad (31)
$$

Here the geometrically weighted average is analogous to the results obtained within the proximity force approximation [40]. This scheme amounts to using the force density obtained from the homogeneous case and integrating over the local contributions of the force densities corresponding to the regions with anchoring energies per area W_a and W_b, respectively. The particular contributions from the regions close to the chemical steps cause deviations from this approximation. Therefore this result holds only for a low number density of chemical steps, i.e., for $d \ll \zeta$.

For intermediate values of d/ζ we have calculated the force $\mathcal{F}$ numerically based on the complete expression given by Eq. (25). In order to highlight the deviation
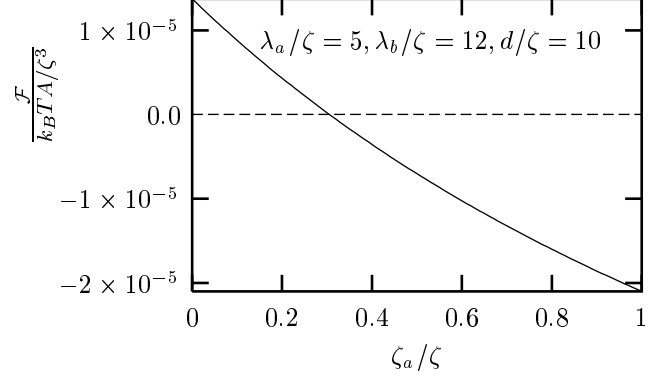

FIG. 4: The fluctuation-induced force $\mathcal{F}$ as a function of the patterning ratio ζ_a/ζ for a fixed reduced separation d/ζ (fulfilling the requirement $d \gg \zeta$, see Fig. 2) and fixed reduced extrapolation lengths $\lambda_{a(b)}/\zeta$ [Eq. (26)]. The crossover from repulsion to attraction indicates that upon increasing ζ_a/ζ the system transforms from the effective strong-weak to the effective strong-strong anchoring regime. For the given set of the parameters ($\lambda_a/\zeta = 5$, $\lambda_b/\zeta = 12$, and $d/\zeta = 10$), the force becomes attractive when more than 31% of the substrate consists of strong anchoring parts with $W_a > W_b$, i.e., $\lambda_a = K/W_a < \lambda_b = K/W_b$. Note that here $\mathcal{F}$ is measured in units of ζ^3 instead of λ_{eff}^3 as in Fig. 2.

of the fluctuation-induced force in the considered patterned system from the long-ranged behavior in the homogeneous cases, we show in Figs. 5 and 6 the rescaled decrease of the force relative to the decay $\sim d^{-3}$ in the repulsion and attraction regime, respectively.

B. Pattern of competing anchoring energies

In the following we generalize the system to a patterned bottom substrate characterized not only by different anchoring strengths but also different preferred molecular axes. We consider a pattern consisting of alternating stripes of either homeotropic or degenerate planar anchoring, i.e., positive values for W_a and negative values for W_b, so that the liquid crystal is subject to competing preferred orientations at the bottom substrate while the upper substrate still exhibits strong homeotropic anchoring. In this case fluctuations are suppressed at the stripes of homeotropic anchoring and enhanced at the stripes of planar anchoring [Eq. (6)]. For those ranges of the model parameters for which the frustrating effect of the interlaced planar anchoring does not modify the mean orientation of the director, the uniform configuration of the director is thermodynamically stable and the system can be described as in the previous subsection. However, if the planar anchoring becomes dominant, the uniform director configuration is destabilized. For this case, we determine the behavior of the fluctuation-induced force before the onset of the ensuing structural phase transi-
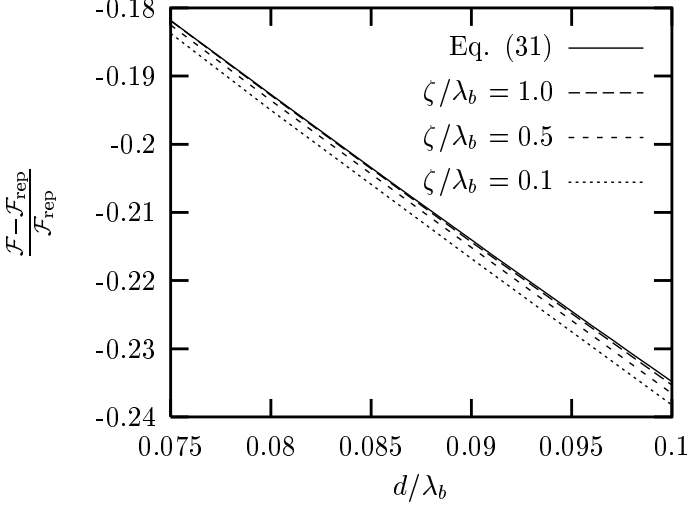
FIG. 5: Rescaled relative decrease of the fluctuation-induced force in the case in which the pattern is characterized by alternating anchoring strengths as a function of the reduced separation d/λ_b compared to the repulsive force $\mathcal{F}_{\text{rep}} = 3k_BTA\zeta(3)/(16\pi d^3)$ between two homogeneous boundaries characterized by infinitely strong and zero anchoring energy, respectively. For $d \ll \zeta$ Eq. (31) holds. Both integrals in Eq. (31) happen to have the same form as in Eq. (26) (which holds, however, for $d \gg \zeta$) with λ_{eff} replaced by λ_a and λ_b, respectively. According to the discussion in the second paragraph following Eq. (26), for the parameter values $\zeta_a = \zeta_b$ and $\lambda_a/\lambda_b = 0.4$ chosen here these integrals are positive for $d/\lambda_b < 0.48$ for the contribution associated with λ_a and $d/\lambda_b < 1.19$ for the contribution associated with λ_b. Thus one expects that on the basis of Eq. (31) $\mathcal{F}$ reduces to $\mathcal{F}_{\text{rep}}$ as given by Eq. (29) for $d/\zeta \to 0$. The solid curve corresponds to $\mathcal{F}$ given by Eq. (31) and the other curves correspond to the full numerical results obtained from Eq. (25) for the indicated values of ζ/λ_b. All curves appear to vanish for $d/\zeta \to 0$ and thus confirm the above expectation. Moreover, by increasing the periodicity the difference between the solid curve and the numerical results vanishes and thus confirms Eq. (31) as a reliable approximation in the limit $d/\zeta \to 0$.

tion.

We consider again first the case $d/\zeta \gg 1$ which allows us to describe the force in terms of an effective anchoring energy and an effective extrapolation length. Within the same approximation as in the preceding subsection, i.e., truncating the matrix B at order $I = 1$, the force [Eq. (25)] is given by

$$\mathcal{F}(d \gg \zeta) = \frac{k_BTA}{\pi d^3} \int_0^\infty dx \frac{x^2}{\frac{x-d/\lambda_{\text{eff}}}{x+d/\lambda_{\text{eff}}} \exp(2x) + 1} \quad (32)$$

where

$$\lambda_{\text{eff}} = \zeta\lambda_a\lambda_b / \mid \zeta_a\lambda_b - \zeta_b\lambda_a \mid \quad (33)$$

and $x = pd$ is the rescaled momentum [41]. The form of this force is that of the force for the hybrid cell [42] with
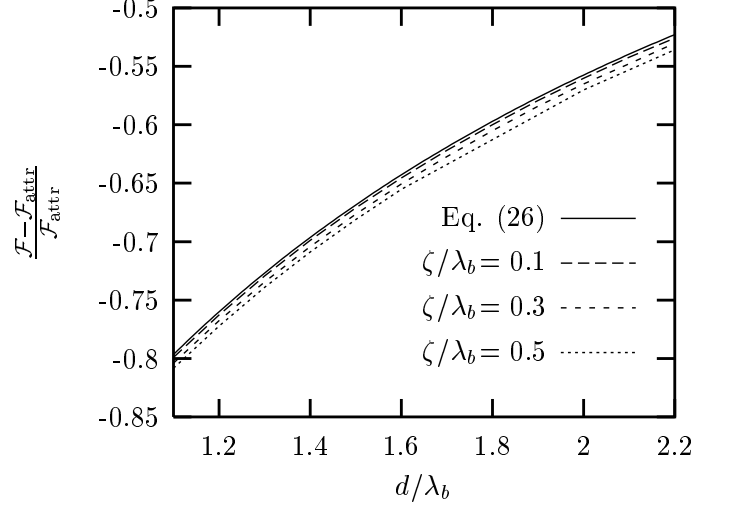

FIG. 6: Rescaled relative decrease of the fluctuation-induced force in the case in which the pattern is characterized by alternating anchoring strengths as a function of the reduced separation d/λ_b compared to the attractive force $\mathcal{F}_{\text{attr}} = -k_BTA\zeta(3)/(4\pi d^3)$ between two homogeneous substrates characterized by infinitely strong anchoring energies. For $d \gg \zeta$ Eq. (26) holds. According to the discussion in the second paragraph following Eq. (26) this integral is negative for $d/\lambda_b > 0.68$ for the parameter values $\zeta_a = \zeta_b$ and $\lambda_a/\lambda_b = 0.4$ chosen here. Thus one expects that $\mathcal{F}$ reduces to $\mathcal{F}_{\text{attr}}$ given by Eq. (30) for $\zeta/d \to 0$. The solid curve corresponds to $\mathcal{F}$ given by Eq. (26) and the other curves correspond to the full numerical results obtained from Eq. (25) for the indicated values of ζ/λ_b. All curves appear to vanish for $\zeta/d \to 0$ and thus confirm the above expectation. Moreover, by decreasing the periodicity ζ the difference between the solid curve and the full numerical results vanishes and thus confirms Eq. (26) as a reliable approximation in the limit $\zeta/d \to 0$.

the bottom substrate described by an effective planar anchoring $W_{\text{eff}} = \zeta_aW_a/\zeta + \zeta_bW_b/\zeta < 0$. Thus in this limit the patterning enters only via this expression for W_{eff}.

For $\zeta \ll d \ll \lambda_{\text{eff}}$ the long-ranged repulsion between the boundaries, characterized by strong and effectively weak anchoring, is enhanced:

$$\mathcal{F}(\zeta \ll d \ll \lambda_{\text{eff}}) \approx \frac{3k_BTA\zeta(3)}{16\pi d^3} \left(1 + \frac{8\ln 2}{3\zeta(3)} \frac{d}{\lambda_{\text{eff}}}\right). \quad (34)$$

Upon approaching the critical separation $d_c = \lambda_{\text{eff}}$ the force increases and, within the Gaussian approximation, diverges logarithmically at d_c:

$$\mathcal{F}(d/d_c \to 1) \approx -\frac{3k_BTA}{4\pi\lambda_{\text{eff}}^3} \left[\ln\left(1 - \frac{d}{d_c}\right) + \ln 2 + ...\right]. \quad (35)$$

This behavior follows from the fact that for $d = \lambda_{\text{eff}}$ the denominator of the integrand in Eq. (32) vanishes as $\frac{2}{3}x^3$ for $x \to 0$. Thus the pretransitional behavior ($d \to d_c$)

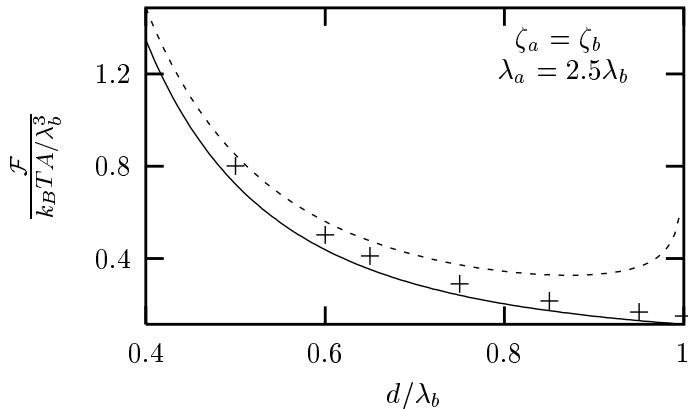FIG. 7: The fluctuation-induced force as a function of the reduced separation d/λ_b in the case in which the pattern is characterized by competing anchoring energies. The solid curve shows the result for small periodicity ($\zeta \ll d$) where the pattern can be described by an effective anchoring energy per area $W_{\text{eff}} = \zeta_a W_a/\zeta + \zeta_b W_b/\zeta < 0$ [Eq. (32)]. The dashed curve shows the result for large periodicity ($\zeta \gg d$) for which the proximity force approximation is valid [Eq. (36)]. The data points (+) show our full numerical results [Eq. (25)] for $\zeta/\lambda_b = 1.5$. This illustrates that as expected $\mathcal{F}$ approaches the proximity force solution (dashed curve) for $d/\zeta \to 0$ and the effective anchoring solution (solid curve) for $d/\zeta \to \infty$.

of the force is related to the sigularity of the soft mode ($x \to 0$).

The logarithmic divergence is a characteristic feature of the perturbative method [Eq. (3)] if applied to a system subject to structural phase transitions [42, 43, 44, 45]. Here the planar anchoring destabilizes the uniform structure governed by the strong homeotropic anchoring at the upper boundary. Upon increasing the separation d the influence of the upper boundary decreases and the destabilizing effect of the substrate characterized by the planar anchoring increases so that upon approaching $d = d_c$ the uniform structure becomes unstable [29]. Beyond the critical separation, the director structure is no longer uniform and the Gaussian Hamiltonian given by Eq. (4) does no longer describe the system. For $d \gtrsim d_c$ one must consider the fluctuations around a nonuniform configuration $\mathbf{n}_0(\mathbf{r})$. It is possible and even likely that the actual critical film thickness for the structural phase transition is not given by $d_c = \lambda_{\text{eff}}$ as obtained in the present perturbative approach.

In the regime of the uniform director configuration, for separations comparable to the periodicity we have calculated the force numerically. As for Eq. (31), in the limit $d/\zeta \ll 1$ the force is given by the geometrically

weighted average of the local force densities:

$$\mathcal{F}(d \ll \zeta) = \frac{k_B T A}{\pi d^3} \left(\frac{\zeta_a}{\zeta} \int_0^\infty \mathrm{d}x \frac{x^2}{\frac{x+d/\lambda_a}{x-d/\lambda_a} \exp{(2x)} + 1} \right.$$
$$\left. + \frac{\zeta_b}{\zeta} \int_0^\infty \mathrm{d}x \frac{x^2}{\frac{x-d/\lambda_b}{x+d/\lambda_b} \exp{(2x)} + 1} \right). \ (36)$$

In Fig. 7 the behavior of the fluctuation-induced force is shown for the three different regimes.

IV. SUMMARY AND CONCLUSION

Based on the Frank [Eq. (1)] and Rapini-Papoular [Eq. (2)] expression for the bulk and surface free energy, respectively, we have studied by field theoretical techniques the contribution of Gaussian fluctuations of the orientational order to the effective force acting on the planar and parallel boundaries of a nematic film of thickness d. The upper boundary exhibits strong and homogeneous homeotropic anchoring whereas the bottom boundary is characterized by a one-dimensional, steplike periodic modulation with period ζ of either the strength or the orientation of the anchoring which is homeotropic or planar (see Fig. 1). The system parameters are chosen such that the thermal average of the nematic order configuration is spatially homogeneous throughout the film. Our main results are the following:

(1) For $d \gg \zeta$, the fluctuation-induced force is proportional to d^{-3} times a scaling function which attains the same form as in the case that the patterned bottom substrate exhibits a homogeneous anchoring energy per area $W_{\text{eff}} = \zeta_a W_a/\zeta + \zeta_b W_b/\zeta$ with the different anchoring energies per area $W_{a(b)} = K/\lambda_{a(b)}$ weighted according to their lateral geometric contribution (Eqs. (26) and (27) as well as (32) and (33)). If a change of the pattern of the anchoring strength causes the corresponding effective boundary condition on the patterned substrate to change from homeotropic weak to homeotropic strong anchoring, the force exhibits a crossover from repulsion to attraction (see Figs. 2, 3, and 4). For a pattern of competing anchoring energies in the case that the stripes with planar anchoring are dominant relative to the stripes of homeotropic anchoring, the fluctuation-induced force is repulsive and nonmonotonic.

(2) For $d \ll \zeta$, the proximity approximation is valid, i.e., the force is given by the geometrically weighted average of the local force densities obtained from the homogeneous substrates (Eqs. (31) and (36)).

(3) For intermediate separations, we have examined the behavior of the force numerically. For a pattern of homeotropic anchoring with alternating strengths, the rescaled relative decrease of the fluctuation-induced force as a function of the reduced separation compared to the long-ranged force is summarized in Figs. 5 and 6 for several values of the reduced periodicity. We note that by increasing the reduced periodicity the system approaches

the limit of the proximity force approximation given by Eq. (31) (solid line in Fig. 5), while by decreasing the reduced periodicity the system approaches the limit of the effective anchoring approximation given by Eq. (26) (solid line in Fig. 6).

(4) For a pattern of competing anchoring energies, the behavior of the force is summarized in Fig. 7. Also in this case the full numerical solution interpolates between the asymptotic formulae given for small d [Eq. (36)] and large d [Eq. (32)].

Besides the force due to fluctuations of the director in a nematic film, there are additional forces acting between interfaces of the film such as the well-known van der Waals dispersion force [24] so that the total force is the sum of the fluctuation-induced and the dispersion forces. In the case that the mean director is inhomogeneous so-called structural forces appear in addition which are not present in the homogeneous case considered here. For a film geometry of thickness d and area A, the dispersion force decays as $-AH/(6\pi d^3)$ where H is the so-called Hamaker constant. As implied by Eqs. (26) and (32),

the magnitude of the fluctuation-induced force scales as $k_B T A/d^3$. Thus, apart from a numerical prefactor of order one, the overall ratio between the dispersion force and the fluctuation-induced force is given by $H/k_B T$. Since liquid crystals and glass substrates have typically comparable indices of refraction, the Hamaker constant is of the order $10^{-21} J$ [46] which is the same order of magnitude as $k_B T$ at room temperature. Therefore typically the dispersion and fluctuation induced force in liquid crystals are of the same order of magnitude and thus comparable. We mention that for a more adequate estimate of the Hamaker constant the anisotropy of the liquid crystal has to be taken into account [47]. For larger thicknesses the dispersion force decays faster ($\sim 1/d^4$) due to retardation [48], so that for sufficiently thick films the fluctuation-induced force dominates.

Finally we note that while the direct measurement of the fluctuation-induced force in liquid crystals has not yet been accomplished, these forces affect in a characteristic way the pattern formation of thin liquid-crystalline dewetting films [49, 50, 51].

---

[*] Electronic address: karimi@fluids.mpi-stuttgart.mpg.de

[1] G. Barbero and G. Durand, J. Phys. II **1**, 651 (1991).

[2] G. Barbero, T. Beica, A. L. Alexe-Ionescu, and R. Moldovan, J. Phys. II **2**, 2011 (1992).

[3] G. P. Bryan-Brown, C. V. Brown, I. C. Sage, and V. C. Hui, Nature **392**, 365 (1998).

[4] G. P. Bryan-Brown, E. L. Wood, and I. C. Sage, Nature **399**, 338 (1999).

[5] G. Barbero, G. Skačej, A. L. Alexe-Ionescu, and S. Žumer, Phys. Rev. E **60**, 628 (1999).

[6] P. Patricio, M. Telo da Gama, and S. Dietrich, Phys. Rev. Lett. **88**, 245502 (2002).

[7] B. Zhang, F. K. Lee, O. K. C. Tsui, and P. Sheng, Phys. Rev. Lett. **91**, 215501 (2003).

[8] H. Yokoyama, S. Kobayashi, and H. Kamei, J. Appl. Phys. **56**, 2645 (1984).

[9] T. Z. Qian and P. Sheng, Phys. Rev. Lett. **77**, 4564, (1996).

[10] T. Z. Qian and P. Sheng, Phys. Rev. E **55**, 7111 (1997).

[11] B. Wen, J-H. Kim, H. Yokoyama, and C. Rosenblatt, Phys. Rev. E **66**, 041502 (2002).

[12] S. Kitson and A. Geisow, Appl. Phys. Lett. **80**, 3635 (2002).

[13] J-H. Kim, M. Yoneya, and H. Yokoyama, Nature **420**, 159 (2002).

[14] S. Kondrat, A. Poniewierski, and L. Harnau, Eur. Phys. J. E **10**, 163 (2003).

[15] A. Sugimura and D. Ishino, Thin Solid Films **438**, 433 (2003).

[16] H. T. A. Wilderbeek, J-P Teunissen, C. W. M. Bastiaansen, and D. J. Broer, Adv. Mater. **15**, 985 (2003).

[17] M. Stalder and M. Schadt, Liq. Cryst. **30**, 285 (2003).

[18] A. Poniewierski and S. Kondrat, J. Mol. Liq. **112**, 61 (2004).

[19] J. Chen, P. J. Bos, D. R. Bryant, D. L. Johnson, S.H. Jamal, and J. R. Kelly, Appl. Phys. Lett. **67**, 1990 (1995).

[20] S. A. Pikin, *Structural transformations in liquid crystals* (Gordon and Breach, Amsterdam, 1991).

[21] R. G. Horn, J. N. Israelachvili, and E. Perez, J. Phys. (France) **42**, 39 (1981).

[22] P. G. de Gennes, Langmuir **6**, 1448 (1990).

[23] P. Ziherl, Phys. Rev. E **61**, 4636 (2000).

[24] J. Israelachvili, *Intermolecular and Surface Forces* (Academic Press, London, 1991).

[25] A. Ajdari, L. Peliti, and J. Prost, Phys. Rev. Lett. **66**, 1481 (1991).

[26] L. Harnau, private communication.

[27] P. G. de Gennes and J. Prost, *The Physics of Liquid Crystals* (Clarendon, Oxford, 1993).

[28] A. Rapini and M. Papoular, J. Phys. Colloq. France **30**, C4-54 (1969).

[29] G. Barbero and R. Barberi, J. Phys. (Paris) **44**, 609 (1983).

[30] The cross terms in the expansion of Eq. (1) in terms of δ_x and δ_y drop out after performing integrations by parts and assuming periodic boundary conditions. In the general case of an anisotropic elastic free energy, the Hamiltonian can be diagonalized in terms of longitudinal and transverse components (see Ref. [25]): $H[\phi_1, \phi_2] = \frac{1}{2}\sum_{i=1}^{2}\int d^3x \left[K_i(\boldsymbol{\nabla}_\perp\phi_i)^2 + K_3(\partial_z\phi_i)^2\right]$ where $\boldsymbol{\nabla}_\perp$ is the nabla operator with respect to the lateral coordinates. Consequently, for this case the result for the force as obtained from Eq. (4) has to be multiplied by $\frac{1}{2}\left(\frac{K_3}{K_1} + \frac{K_3}{K_2}\right)$.

[31] H. W. Diehl, in *Phase Transitions and Critical Phenomena*, edited by C. Domb and J. L. Lebowitz (Academic Press, London, 1986), Vol. 10, p. 75.

[32] H. Li and M. Kardar, Phys. Rev. Lett. **67**, 3275 (1991).

[33] R. Golestanian and M. Kardar, Phys. Rev. A **58**, 1713 (1998).

[34] P. M. Chaikin and T. C. Lubensky, *Principles of condensed matter physics* (Cambridge University Press, Cambridge, 1995).

[35] T. Emig, Europhys. Lett. **62**, 466 (2003).

[36] R. Büscher and T. Emig, preprint cond-mat/0401451.

[37] Note however, that there are cases such as the hybrid cell studied in Ref. [42] in which the surface and the finite-size free energies cannot be disentangled for long wavelength modes.

[38] P. Ziherl, R. Podgornik, and S. Žumer, Chem. Phys. Lett. **295**, 99 (1998).

[39] P. Ziherl and I. Muševič, Liq. Cryst. **28**, 1057 (2001).

[40] B.V. Derjaguin, I.I. Abrikosova, and E.M. Lifshitz, Quart. Rev. **10**, 295 (1956).

[41] We exclude here the case of tilted easy directions for which the director structure might not be uniform and, therefore, the formalism introduced here cannot be applied.

[42] P. Ziherl, F. Karimi Pour Haddadan, R. Podgornik, and S. Žumer, Phys. Rev. E **61**, 5361 (2000).

[43] F. Karimi Pour Haddadan, D. W. Allender, and S. Žumer, Phys. Rev. E **64**, 061701 (2001).

[44] N. Uchida, Phys. Rev. Lett. **87**, 216101 (2001).

[45] B. Markun and S. Žumer, Phys. Rev. E **68**, 021704 (2003).

[46] K. Kočevar and I. Muševič, Phys. Rev. E **64**, 051711 (2001).

[47] A. Šarlah and S. Žumer, Phys. Rev. E **64**, 051606 (2001).

[48] J. Chen and A. Anandarajah, J. Colloid Interface Sci. **180**, 519 (1996).

[49] D. van Effenterre, R. Ober, M. P. Valignat, and A. M. Cazabat, Phys. Rev. Lett. **87**, 125701 (2001).

[50] S. Schlagowski, S. Herminghaus, and K. Jacobs, Europhys. Lett. **57**, 519 (2002).

[51] P. Ziherl and S. Žumer, Eur. Phys. J. E **12**, 361 (2003).